— Supplementary Information —

High-T_c superconductors as a New Playground for High-order Van Hove singularities and Flat-band Physics

Robert S. Markiewicz,[1,*] Bahadur Singh,[2,†] Christopher Lane,[3,4] and Arun Bansil[1]

[1] Department of Physics, Northeastern University, Boston, Massachusetts 02115, USA
[2] Department of Condensed Matter Physics and Materials Science, Tata Institute of Fundamental Research, Colaba, Mumbai 400005, India
[3] Theoretical Division, Los Alamos National Laboratory, Los Alamos, New Mexico 87545, USA
[4] Center for Integrated Nanotechnologies, Los Alamos National Laboratory, Los Alamos, New Mexico 87545, USA

S-I. VAN HOVE DICHOTOMY

S-I.A. Van Hove dichotomy at the VHS, vs t'

In the main text, we have considered VHSs with diverging $q = 0$ susceptibility. However, the VHS also has a diverging susceptibility at a second wave momentum Q near (π, π) as well. This is resolved in Fig. S1 where the variation of t' shifts the dominant susceptibility peak from (π, π) to $\Gamma = (0, 0)$ as $-t'$ increases. Similar effects arise as doping x increases from 0. This dichotomy is very relevant for cuprate physics since only the VHS near (π, π) is correlated with the pseudogap crossover temperature, $T_Q \simeq T_{pg}$. We now demonstrate how these two VHSs compete and evolve with t' and x.

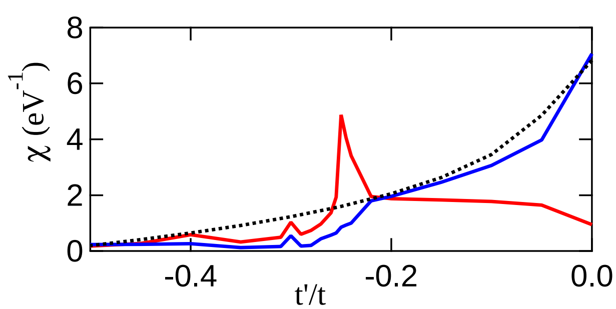

FIG. S1. Competition between near-(π, π) (blue line) and Γ-VHSs (red line), for t''/t' = -0.5. Black dotted line indicates analytic approximation for the former.

In this connection, we calculate the full DFT-Lindhard susceptibility,

$$\chi_0(q, \omega) = -\sum_k \frac{f(\epsilon_k) - f(\epsilon_{k+q})}{\omega - \epsilon_{k+q} + \epsilon_k} \quad \text{(S1)}$$

The real part of $\chi_0(q, \omega = 0)$ contains two contributions: the diverging peaks associated with VHS nesting[1] plus a folded ($q = 2k_F$) map of the Fermi surface, whose intensity quantifies the strength of Fermi surface nesting. The susceptibility is not confined to the Fermi surface, but contains a substantial bulk contribution which can favor certain k_F values, or even shift the peak to a nearby commensurate value, necessitating a careful numerical evaluation of χ_0.[2]

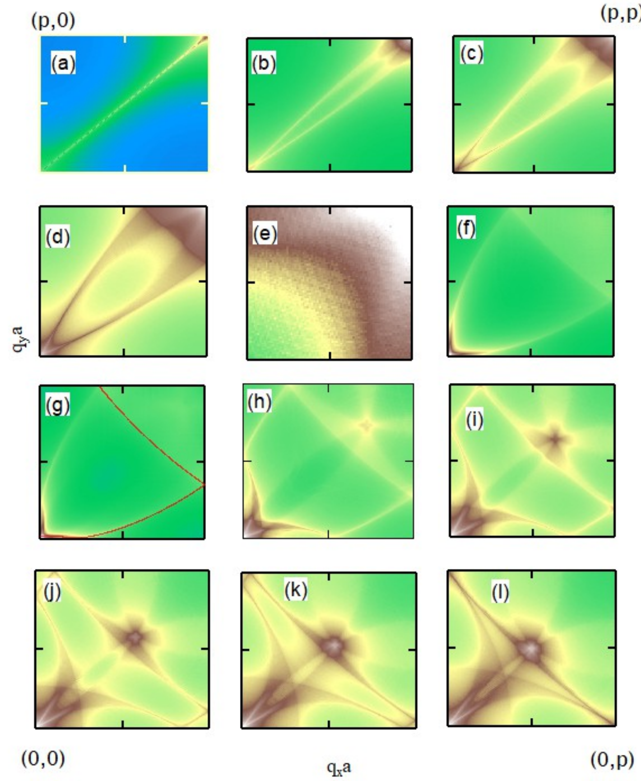

FIG. S2. Susceptibility maps at saddle-point VHS for t'/t = (a) 0.0, (b) -0.05, (c) -0.10, (d) -0.15, (e) -0.20, (f) -0.25, (g) -0.258 [Bi2201], (h) -0.30, (i) -0.35, (j) -0.40, (k) -0.45, and (l) -0.50. Blue and white identify minimum and maximum intensities, respectively.

Figure S2 shows the evolution of the susceptibility at the VHS doping as t' is varied, keeping $t'' = -0.5t'$, which is thought to be relevant to the cuprates. In Fig. S2(g), we show the Fermi surface nesting curve $q = 2k_F$ (red line) over part of the first Brillouin zone. This clearly identifies that the nonanalytic features of the susceptibility are associated with Fermi-surface nesting. It can be seen that for each $|t'|$, there are susceptibility divergences at Γ and (π,π), due to intra- and inter-VHS scattering, respectively. However for small $|t'|$, the more intense VHS feature is at (π,π) whereas for larger $|t'|$, the peak at Γ becomes most intense. From Fig. S1, we note that the crossover occurs near $t' = -0.2t$, pinned by the high-order VHS peak. For intermediate values of $|t'|$, there is an additional peak at $(\pi-\delta, \pi-\delta)$ (see Fig. S2(h) for example).

To understand the (π,π) VHS evolution, we recall that for the pure Hubbard model ($t' = 0$), the (π,π)-susceptibility has a log^2T divergence that reduces to

$$\chi((\pi,\pi),0) \sim log(T)log(T_X),$$

where $T_X = max\{T, T_{eh}\}$ and $k_BT_{eh} = |t'|$, for finite t'.[3] The dotted black line in Fig. S1 is proportional to $ln(|t'|)$ (with an effective t' at $t' = 0$, to account for the finite k-mesh), showing that this is a good approximation over a broad range of t', even in the presence of $t'' \neq 0$.

Near the high-symmetry points, the susceptibility peak can deviate from the nesting map. This can be understood by taking the symmetry point (π,π) as an example. While the susceptibility at Γ is constrained to be a Fermi surface effect, for general q there can be a strong contribution to χ_0 from states far from E_F, leading to peaks with very broad tails. These tails play an important role near high-symmetry points, when multiple Fermi surface sections approach the symmetry point. Figure S2 illustrates this effect for the (π,π) plateau. For larger $|t'|$, Figs. S2(f)-(l), the weight is concentrated near the nesting map, $q = 2k_F$. However, as $|t'|$ decreases, overlap of the bulk spectral weight rapidly shifts the peak to exactly (π,π), as the plateau shrinks down to a point for $t' = 0$ (Fig. S2(a)). Similar overlap effects explain why the susceptibility peaks near Γ can shift away from the nesting map.

The pileup of states at (π,π) for small $|t'|$ has two consequences- first, a prominent commensurate-incommensurate transition[2], and second, the rapid decrease of intensity at (π,π) with increasing $|t'|$ seen in Fig. S1. We note that the Fermi surfaces responsible for the $q \sim (\pi,\pi)$ plateau come from $k_F \sim (\pi/2,\pi/2)$ – i.e., far from the VHS and hence not sensitive to t''. Indeed, the t'-dependence of the (π,π) plateau area, Fig. S2, is qualitatively similar to the doping dependence of the plateau area at fixed t', Fig. S3.

S-I.B. Van Hove dichotomy vs doping at fixed t': Tuning away from the VHS

While the t' dependence of the VHS susceptibility is easy to calculate, since only the doping x_{VHS} is involved, the doping dependence at fixed t' (i.e., for a particular cuprate) is often more important. This is more complex since, for $x \neq x_{VHS}$, each VHS evolves into a finite susceptibility peak with different doping dependence. We illustrate this evolution in Figure S3 for a typical $t'/t = -0.3$. The susceptibility has a number of nonanalytic peaks, associated with Fermi surface nesting. To illustrate this, we include superposed maps of the main barrel Fermi surfaces, doubled and folded back to the first Brillouin zone (BZ), to highlight the $q = 2k_F$ nesting features.[2] Additional features in frames (f-h) are associated with non-$2k_F$ nesting,[2,4], e.g., inter-Fermi surface pocket nesting as illustrated in frame (b) for the doping of frame (g).

To better understand the structure in these susceptibility maps, we briefly review the evolution of the Fermi surface, and its two topological transitions[2,4]. Figure S3(a) shows the corresponding DOS, with points at which the susceptibility maps were sampled. The DOS has two VHSs – a logarithmic peak where a pocket pinches off near $(\pi, 0)$, frame (f), and a step down when the pocket disappears with further hole doping, frame (h). Due to the folding, the pockets appear near Γ in the susceptibility maps.

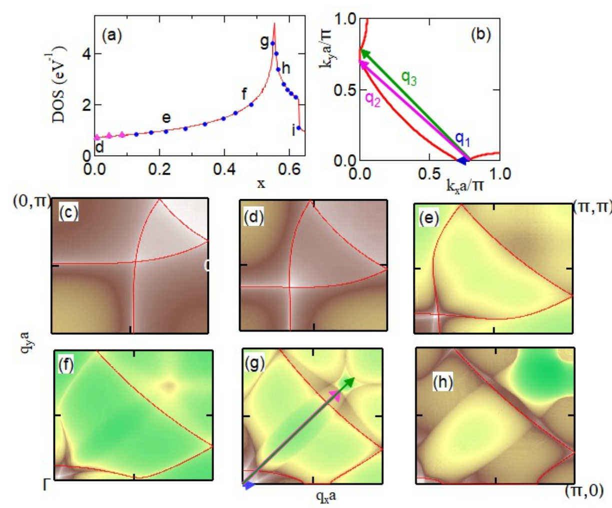

FIG. S3. **Susceptibility maps showing evolution of nesting lines with doping for $t'/t = -0.3$, $t''/t' = -0.5$.** (a) DOS, showing doping of each susceptibility map. (b) Fermi surface for frame (g) showing three inter-surface nesting vectors. (c-h) Susceptibility maps, with $q = 2k_F$ nesting surface superposed as a red line; in frames (f-h), one branch is omitted to emphasize details of the nesting maps. Color scheme same as Fig. S2. In frames (c-h), the (π,π)-plateau is defined as the area enclosed by the folded Fermi surface nearest to (π,π). Arrows in (g) match those in (b).

For present purposes, our main result is to see how the VHS competition plays out as the Fermi level is shifted away from E_{VHS}. As doping x increases, the dominant nesting vector shifts away from $(\pi,\pi-\delta)$ at low doping (violet triangles in frame (a)) to (δ',δ'), or antinodal nesting (ANN), at higher doping (blue dots), near $x_{cross} \sim 0.12$. Experimentally, the peak at $(\pi,\pi-\delta)$ is associated with an incommensurate SDW, while the ANN peak drives a CDW instability. As the VHS peak is approached, the ANN peak flows to Γ, $\delta' \to 0$ at the VHS, while the peak at $(\pi, \pi-\delta)$ evolves to a weak peak at $(\pi-\delta'', \pi-\delta'')$ at the VHS, green circle in Fig. S3(f). Thus we have demonstrated that this competition is controlled by the competition between intra-VHS scattering near Γ and the inter-VHS scattering near (π,π). That is, the VHSs are important not only at x_{VHS}, but influence the dominant susceptibility over a wide doping range.

The peak crossover seen at $x_{cross} = 0.12$ in Fig. S3 is reflected in a similar crossover of the VHS peaks, Fig. S1, at $t'_{cross} \sim -0.2$, for $t'' = -0.5t'$. For all $t' > t'_{cross}$ there is no x_{cross} and the (π,π)-VHS is always dominant, while for $t' < t'_{cross}$ there is always an x_{cross} where the influence of the (π,π)-VHS is lost. Note that in the example of Fig. S3, $x_{cross} = 0.12 << x_{VHS} = 0.54$.

S-II. NEW ln^2T VHSS

In this Section, we propose a further generalization of higher-order VHSs, in which the faster-than-logarithmic divergence is not in the DOS, but in a competing, finite-q susceptibility. At present, the only known example is the original Hubbard model, $t' = t'' = 0$, with a $ln^2(T)$ $q = (\pi,\pi)$ susceptibility divergence. Here, we demonstrate that it is not unique by generating a family of dispersions with this property. As a byproduct, we demonstrate an improved technique for generating tight-binding models, in which the hopping parameters are approximately orthogonal.

Here, we generalize the analysis of Ref. 3 for finite t''. The susceptibility divergence arises from the energy integral in Eq. S1, with ϵ_k near, e.g., $(\pi,0)$, while ϵ_{k+Q} is near $(0,\pi)$. For the $t-t'-t''$ model, the t' and t'' terms cancel, and the denominator becomes $\epsilon_k - \epsilon_{k+Q} = -4t(c_x + c_y)$. Near $(0,\pi)$, $c_x + c_y \sim k_x^2 - k_y'^2 \sim k^2 cos(2\phi)$, with $k'_y = \pi - k_y$. Then the integral $\int kdk/k^2$ produces a logarithmic divergence, which can be cut off by, e.g., the temperature T. The angle integral $\int d\phi/cos(2\phi)$ also can diverge, if $\phi \to \pi/4$, leading to a second $ln(T)$ factor. However, the fermi functions in Eq. S1 can cut off this divergence, since at low T they only allow scattering from full to empty states, and hence cut the ϕ integral off at the Fermi surface. To test this possibility, we rewrite Eq. 1 by using $cos(2\theta) = 2cos^2(\theta) - 1$, as

$$\epsilon_k = -2t(c_x+c_y) - (t'+2t'')(c_x+c_y)^2 + (t'-2t'')(c_x-c_y)^2 + 4t''. \quad \text{(S2)}$$

Thus, when $t'' \neq 0$, the cutoff of Eq. S2 becomes $k_BT_{eh} = |t' - 2t''|$, and when $2t'' = t'$, the susceptibility has a $ln^2(T)$-divergence independent of $t' + t''$, leading to a new reference family of anomalous VHSs, Fig. S4.

Figure S4 shows that the dispersion changes strongly with t', whereas the contours of constant energy are independent of t', since they represent $c_x + c_y = R =$ *constant*. Consequently, for all values of t', the zone diagonal $(0,\pi) \to (\pi,0)$ lies at the VHS, $E_F = E_X$, ensuring a square Fermi surface and a $ln^2(T)$-divergence of the (π,π) susceptibility. However, there is still a competition of (π,π) and Γ susceptibilities, except now in terms of high-order VHSs. Note that for $t' = 0$ (the conventional Hubbard model) the dispersion is electron-hole symmetric. For $t' < 0$, the dispersion becomes asymmetric, with a local peak developing at Γ, leading to a Mexican hat potential, which moves toward the $(0,\pi) \to (\pi,0)$ line as $|t'|$ increases. The minimum of the Mexican hat produces a flat band quite similar to that found in secondary high-order VHSs.

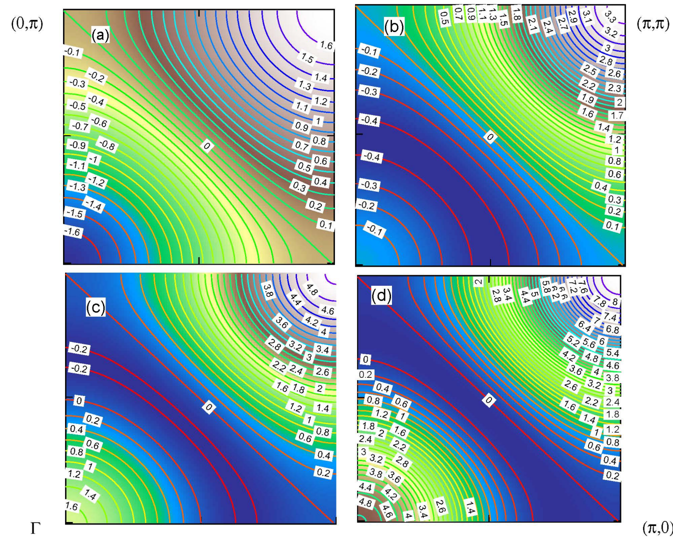

FIG. S4. **Dispersion maps $E - E_X$ showing evolution of constant energy surfaces with t' for $t''/t' = 0.5$.** $t'/t =$ (a) 0, (b) -0.5, (c) -1, and (d) -0.2. Constant energy contours are labeled in eV.

This similarity is not accidental. For a mean-field model of $Q = (\pi,\pi)$ AFM order, the dispersion in the AFM phase becomes $E_\pm = \epsilon_+ \pm \sqrt{\epsilon_-^2 + U^2/4}$, where $\epsilon_\pm = (\epsilon_k \pm \epsilon_{k+Q})/2$. When U is large, the square-root term becomes $U/2 + \epsilon_-^2/U$. In the $t - t' - t''$ families, $\epsilon_- = -2t(c_x + c_y)$, and the square-root term becomes $U/2 + J(c_x + c_y)^2$, $J = 4t^2/U$, having the same nonlinear term as Eq. S2.

Thus, remarkably, whereas the DOS is highly sensitive to the Fermi surface, the $q = (\pi,\pi)$ susceptibility obeys the simpler result of Eq. S2, and can only have ln or ln^2 divergences in the (π,π) susceptibility. We note that the original Hubbard model required extreme fine tuning (all hopping parameters except t equal to zero), calling into question the relevance of a square Fermi surface and resultant ln^2 divergence. By showing that a square Fermi surface can be found along an entire cut in parameter space, we have greatly enhanced the likelihood that such a feature, with accompanying high-order VHSs, might be experimentally observed.

Finally, we have defined our parameter space in terms of just the three nearest-neighbor hopping parameters, and for this to be of value, it is necessary that higher-order hopping parameters have negligible effects in most cases. This new, 'Hubbard' family offers a simple test: can a line of square-Fermi-surface states persist as higher order hopping parameters are included? We explore this issue by looking at the most general TB model with terms of order c_i^3 (E_3) and c_i^4 (E_4), $\epsilon_{k,4} = \epsilon_k + E_3 + E_4$. Here ϵ_k is given by Eq 1 and

$$E_3 = -2t_3(c_{3x} + c_{3y}) - 4t_4(c_{2x}c_y + c_{2y}c_x)$$

$$= 2a_3(c_x + c_y) - 4A_3(c_x + c_y)^3 - 4B_3(c_x - c_y)^3, \quad \text{(S3)}$$

with $a_3 = t_3 + 6t_4$, $A_3, B_3 = t_3 \pm t_4/3$,

$$E_4 = -2t_5(c_{4x} + c_{4y}) - 4t_6(c_{3x}c_y + c_{3y}c_x) - 4t_7c_{2x}c_{2y}$$

$$= e_{40} - a_4(c_x+c_y)^2 - b_4(c_x-c_y)^2 - 2A_4(c_x+c_y)^4 - 2B_4(c_x-c_y)^4$$

$$-4C_4(c_xc_y)^2, \quad \text{(S4)}$$

with $e_{40} = -4(t_5 + t_7)$, $a_4, b_4 = 4(t_5 + t_7) \mp 3t_6$, $A_4, B_4 = 4t_5 \pm t_6$, $C_4 = 4(t_7 - 6t_5)$. Finally, since $c_xc_y = [(c_x + c_y)^2 - (c_x - c_y)^2]/4$, $\epsilon_{k,4}$ can be written as a polynomial in $(c_x + c_y)$ and $(c_x - c_y)$. Eliminating all the terms in $(c_x - c_y)$ leaves behind a polynomial in $(c_x + c_y)$, a 4th order generalization of the Hubbard reference family.

We note in passing that our new series expansion, a Taylor series in the two variables $X = c_x + c_y$ and $Y = c_x - c_y$, should be a significant improvement over the conventional neighbor-by-neighbor tight-binding model. We see from Eqs. S3 and S4 that each additional neighbor introduces two kinds of corrections: new terms in X and Y (terms whose coefficients are capital letters on right-hand side of equations) and renormalizations of lower-order terms (terms with lower-case coefficients). In contrast, the new series is essentially a symmetry-corrected Fourier series, ensuring that the new terms added at each order are orthogonal to the lower-order terms, and will be accepted only if they genuinely improve the fit to the dispersion. Moreover, the even order terms are electron-hole symmetric while odd-order terms are not. Only the latter contribute to shifting the VHS from half-filling.

* r.markiewicz@northeastern.edu
† bahadur.singh@tifr.res.in

[1] T. M. Rice and G. K. Scott, New Mechanism for a Charge-Density-Wave Instability, Phys. Rev. Lett. 35, 120 (1975).
[2] R.S. Markiewicz, J. Lorenzana, G. Seibold, and A. Bansil, Gutzwiller magnetic phase diagram of the cuprates. *Phys. Rev. B*81, 014509 (2010).
[3] R.S.Markiewicz, A survey of the Van Hove scenario for high-T_c superconductivity with special emphasis on pseudogaps and striped phases *J. Phys. Chem. Sol.* **58,** 1179 (1997).
[4] R.S. Markiewicz, J. Lorenzana, and G. Seibold, Gutzwiller magnetic phase diagram of the undoped t–t'–U Hubbard model *Phys. Rev. B*81, 014510 (2010).